SCIENCE CHINA
Information Sciences

• RESEARCH PAPER •

June 2024, Vol. 67, Iss. 6, 162303:1–162303:14
https://doi.org/10.1007/s11432-023-3970-7

Near-field wideband beam training for ELAA with uniform circular array

Yuhao CHEN & Linglong DAI*

Department of Electronic Engineering, Tsinghua University, Beijing National Research Center for Information Science and Technology (BNRist), Beijing 100084*, China*

Received 21 August 2023/Revised 24 December 2023/Accepted 5 March 2024/Published online 24 May 2024

Abstract Extremely large-scale antenna array (ELAA) at millimeter wave (mmWave) and Terahertz (THz) band has been considered a key technology for combating high attenuation in high-frequency bands in future 6G communications. Uniform circular arrays (UCAs) have attracted much attention because of their ability to provide flat beamforming gain at all angles. To realize efficient beamforming, beam training is widely used to acquire channel state information. However, with a large antenna number, the beam training overhead in ELAA systems becomes overwhelming. Moreover, with a large bandwidth, the beam defocus effect severely degrades beam training accuracy. To address these issues, this paper proposes a frequency-dependent focusing (FDF)-based beam training scheme to realize effective beam training in near-field wideband ELAA systems with UCA. Specifically, we first analyze the FDF property of UCA, where signals at different subcarriers can simultaneously focus on different distances. Then, by exploiting the FDF property to search different distances using different subcarriers simultaneously, we design a hierarchical codebook and propose an FDF-based beam training scheme. To reveal the effectiveness of the proposed scheme, we compare its necessary beam training overhead with that of existing schemes. Finally, the simulation results demonstrate that the proposed scheme can achieve accurate beam training in near-field wideband UCA systems with a low beam training overhead.

Keywords extremely large-scale antenna array (ELAA), uniform circular array (UCA), near-field, wideband, beam training

1 Introduction

The ever-increasing demand for communication capacity in 6G networks has resulted in a rapid increase in the dimensions of wireless signals in spatial and frequency domains [1]. In the spatial domain, the massive multiple-input-multiple-output (mMIMO) in 5G is evolving to an extremely large-scale antenna array (ELAA) in 6G, which is expected to yield a 10-fold increase in spectral efficiency [2,3]. Meanwhile, in the frequency domain, high-frequency communications operating at millimeter-wave (mmWave) or Terahertz (THz) bands are anticipated to provide richer spectral resourses [4–6]. The high beamforming gain realized by the ELAA can compensate for the high attenuation of high-frequency signals. The integration of ELAA and high-frequency communications is, therefore, natural and is considered to be a key technology for future 6G communications.

Accurate channel state information (CSI) is an essential prerequisite for efficient beamforming in high-frequency ELAA communication systems [7]. Beam training has been widely used to acquire CSI in high-frequency systems [8, 9]. Instead of estimating the entire channel matrix, beam training only identifies the location of the user equipment (UE). Because of the quasi-optical characteristics of high-frequency channels, near-optimal achievable data rate performance can be realized by transmitting pencil beams to the location of UE [10]. In traditional far-field beam training, a codebook predefines a series of beams, each of which focuses the signal energy on different angles in space. Then, by sequentially transmitting the beams, the location of the UE can be obtained according to the codeword with the maximum received power. However, in ELAA systems, an increase in the antenna number causes two

* Corresponding author (email: daill@tsinghua.edu.cn)

problems. First, the large number of antennas sharply increases the number of candidate beams. Second, the large array aperture leads to the extension of the near-field region. In near-field communications, a spherical wavefront should be considered. Because beamforming with a spherical wavefront is related to both angle and distance, the acquisition of distance is essential for near-field beamforming, which adds a new dimension to near-field beam training [11–13]. Near-field beams can be used to search different angles and distances exhaustively, but the number of candidate beams will further increase. These two problems collectively cause an unacceptable beam training overhead in high-frequency ELAA communication systems.

1.1 Prior work

Several studies have been devoted to reducing the beam training overhead in near-field communications, which can be divided into two categories: narrowband beam training [14–18] and wideband beam training [19]. For narrowband scenarios, unlike the exhaustive scheme, authors in [14] designed a multiresolution codebook based on the Gerchberg-Saxton algorithm and proposed the corresponding near-field two-dimensional hierarchical beam training scheme. The accurate location of the UE can be determined by first employing a wide beam to perform a coarse search and gradually reducing the angle and distance ranges layer by layer. Because the hierarchical search procedure avoids the inefficient exhaustive search, the beam training overhead can be significantly reduced. Similarly, authors in [15] proposed a spatial-chirp beam-aided codebook to realize hierarchical beam training. By analyzing the beam pattern of the spatial-chirp beam in the slope-intercept domain, the relationship between the angle and the distance can be exploited to reduce the beam training overhead. In addition to searching the entire space layer by layer, some studies have exploited the relationship between traditional far-field codewords and near-field channels to reduce the beam training overhead [16, 17]. Specifically, the authors in [16] proposed a two-phase beam training scheme. In the first phase, the candidate angles of the UE were determined based on the traditional far-field codebook. Then, a customized near-field codebook based on the first phase search was used to determine the location of the UE. Consequently, the beam training overhead of the second phase can be reduced because the first phase remarkably tailors the candidate beams of the UE. In addition, the authors in [17] proposed a deep learning-based beam training scheme, where the far-field wide beams were first transmitted. Then, based on the received signals of the far-field wide beams, a convolutional neural network (CNN)-based network was applied to determine the optimal near-field codeword directly by learning the complex relationship between received energy with the far-field beam and the user location. Thus, no extra codewords are required to estimate the UE distance, and the beam training overhead can be significantly reduced. Similar deep learning schemes have also been studied in [18] to realize an effective beam training.

The schemes described in [14–18] are only suitable for narrowband scenarios. When the bandwidth becomes large, the severe issue of near-field beam split effect appears, where beams at different subcarriers split into different locations [20]. Therefore, in near-field wideband systems, the above narrowband beam training schemes will suffer severe accuracy degradation. To cope with this problem, the authors in [19] revealed the mechanism of the near-field rainbow effect to exploit the beam split effect to search the entire space effectively. By employing the time-delay beamforming in the wideband system, different subcarriers could focus on different pre-designed locations. Thus, the entire space can be searched more effectively, significantly reducing the beam training overhead.

The above near-field beam training schemes for narrowband and wideband systems are only applicable to a uniform linear array (ULA). Nevertheless, in ULA systems, the array gain degrades dramatically near the end-fire because of the reduced effective array aperture [11]. To cope with this drawback, recently, uniform circular array (UCA) has attracted increased attention [21–24]. The UCA can provide flat array gain at different angles in space because of axial symmetry. Furthermore, given a fixed array aperture, the near-field region of the UCA is larger than that of the ULA. Therefore, the advantages of near-field communications (e.g., increased spatial degrees of freedom for single-user communications [25] and newly available resources to increase the spectral efficiency for multiuser communications [26]) can be exploited more efficiently to improve the system capacity. Recently, for the near-field beam training in UCA systems, the authors in [27] designed a near-field codebook for UCA, which revealed that the codebook size of UCA is smaller than that of ULA. However, the beam training scheme in [27] is only suitable for narrowband systems. In wideband systems, the newly investigated beam defocus effect is introduced, where subcarriers at noncentral frequencies cannot form high-gain beams at the intended location [28].

This effect in UCA systems leads to a severe loss in beamforming performance and dramatically decreases the beam training accuracy of the narrowband beam training scheme in [27]. To the best of our knowledge, effective beam training in near-field wideband UCA systems has not yet been investigated.

1.2 Our contributions

To fill this gap, in this paper, we propose a frequency-dependent focusing (FDF)-based beam training scheme to realize effective beam training in near-field wideband ELAA systems with UCA. Specifically, our contributions are listed as follows:

- First, we reveal and analyze the FDF properties in wideband UCA systems. Although the signals of subcarriers at noncentral frequencies cannot focus in the far field, they can still focus on a certain distance in the near field. The FDF property provides an insight into the relationship between the subcarrier frequency and the focusing distance, which inspires us to search different distances with different subcarriers simultaneously. Thus, once the UE angle is determined, the distance domain introduced by the spherical wavefront in near-field communications no longer requires extra beam training overhead.
- Then, an FDF-based beam training scheme is proposed based on the above FDF property. We first designed a two-layer hierarchical codebook to effectively determine the UE angle. In the first layer, the UCA is divided into several subarrays, where each subarray generates beams to search for angles close to its normal direction simultaneously. After first-layer searching, the candidate beams can be significantly tailored. For the second layer, narrow beams with high angular resolutions are generated to estimate the UE angle. After determining the direction, the codeword with the maximum received power is selected to estimate the UE distance. To guarantee a better anti-noise capacity, we propose a subcarrier grouping criterion, in which subcarriers in the same group focus on similar distances and can be combined for analysis. After grouping the subcarriers, the UE distance can then be estimated by exploiting the FDF property analyzed above.
- Finally, we analyze the necessary beam training overhead of the proposed FDF-based beam training scheme and demonstrate that the overhead of the proposed scheme is much lower than that of existing schemes. Simulations are also conducted to verify the advantages of the proposed scheme, which reveals that the proposed scheme can realize a 30% improvement in the achievable rate performance compared with existing schemes with a low beam training overhead.

Organization. The remainder of the paper is organized as follows. In Section 2 introduces the system model for near-field wideband UCA systems. In Section 3, we first analyze the FDF property in wideband UCA systems. Next, we elaborate on the design of the hierarchical codebook and propose an FDF-based beam training scheme. An analysis of the beam training overhead is also conducted. Section 4 provides the simulation results, and the conclusions are presented in Section 5.

Notations. Lower-case and upper-case boldface letters represent vectors and matrices, respectively; $\boldsymbol{x}[a:b]$ represents the a-th element to the b-th element of vector $\boldsymbol{x}$; $(\cdot)^{\mathrm{T}}$ and $(\cdot)^{\mathrm{H}}$ denote the transpose and conjugate transpose, respectively; $|\cdot|$ denotes the absolute value operator; $\|\cdot\|_2$ denotes the 2-norm operator; $\odot$ denotes the Hadamard product operator; $\lceil\cdot\rceil$ denotes the ceiling operator; $\lfloor\cdot\rfloor$ denotes the floor operator; $\mathcal{CN}(\mu,\Sigma)$ and $\mathcal{U}(a,b)$ denote the Gaussian distribution with mean μ and covariance Σ, and the uniform distribution between a and b, respectively.

2 System model

We consider a downlink communication system, where the base station (BS) is equipped with an N-element UCA and the UE is equipped with a single antenna. As illustrated in Figure 1, the antennas at the BS are uniformly distributed along the circle with the radius of R. The orthogonal frequency division multiplexing (OFDM) with M subcarriers is employed in the system, and the bandwidth is set to B. For the m-th subcarrier, the received signal at the UE can be represented as

$$y_m = \boldsymbol{h}_m^{\mathrm{H}}\boldsymbol{w}s_m + n_m, \tag{1}$$

where $\boldsymbol{h}_m \in \mathbb{C}^{N\times 1}$ denotes the channel at the m-th subcarrier, and $\boldsymbol{w} \in \mathbb{C}^{N\times 1}$ denotes the beamforming vector, respectively. The transmitted signal at the m-th subcarrier is denoted by s_m and the noise n_m satisfies $n_m \sim \mathcal{CN}(0,\sigma^2)$ with σ^2 being the noise power.

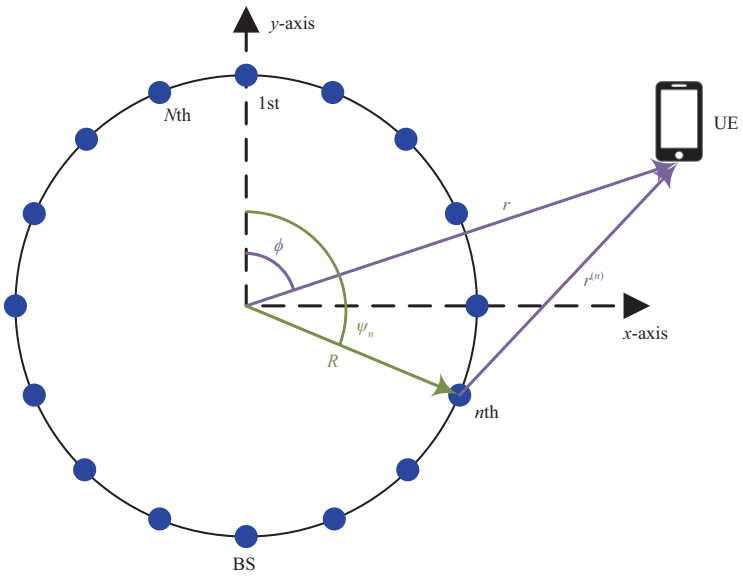

Figure 1 (Color online) System model of the UCA near field communication.

Due to the severe path loss incurred by the scatterers, mmWave and THz communications rely heavily on the line-of-sight (LoS) path [4], so we consider the near-field LoS channel in this paper. Specifically, the channel at the m-th subcarrier $\boldsymbol{h}_m$ can be represented as

$$\boldsymbol{h}_m = \sqrt{N} g_m \mathrm{e}^{-\mathrm{j}\frac{2\pi}{c} f_m r} \boldsymbol{a}_m(\phi, r), \tag{2}$$

where $f_m = f_c + \frac{B}{M}(m - 1 - \frac{M-1}{2})$ denotes the frequency of the m-th subcarrier with f_c being the central frequency, r denotes the distance between the BS and the UE, ϕ denotes the UE angle, and c denotes the speed of light, respectively. The free-space gain g_m can be obtained by $g_m = \frac{f_m}{4\pi c r}$ [29]. The near-field array response vector at the m-th subcarrier $\boldsymbol{a}_m(\phi, r)$ can be elaborated as

$$\boldsymbol{a}_m(\phi, r) = \frac{1}{\sqrt{N}} \left[\mathrm{e}^{-\mathrm{j}\frac{2\pi f_m}{c}(r^{(1)} - r)}, \ldots, \mathrm{e}^{-\mathrm{j}\frac{2\pi f_m}{c}(r^{(N)} - r)} \right]^{\mathrm{T}}, \tag{3}$$

where $r^{(n)}$ represents the distance between the UE and the n-th antenna of UCA, which can be derived as

$$r^{(n)} = \sqrt{r^2 + R^2 - 2rR\cos(\phi - \psi_n)} \overset{\text{(a)}}{\approx} r - R\cos(\phi - \psi_n) + \frac{R^2}{2r}\left(1 - \cos^2(\phi - \psi_n)\right), \tag{4}$$

where $\psi_n = \frac{2\pi n}{N}$ and (a) is obtained according to the second-order Taylor series expansion $\sqrt{1+x} = 1 + \frac{x}{2} - \frac{x^2}{8} + \mathcal{O}(x^2)$. Combining the received signals of all subcarriers, the received signals at the UE can be formulated as

$$\boldsymbol{y} = (\boldsymbol{H}\boldsymbol{w}) \odot \boldsymbol{s} + \boldsymbol{n}, \tag{5}$$

where $\boldsymbol{y} = [y_1, y_2, \ldots, y_M]^{\mathrm{T}}$, $\boldsymbol{H} = [\boldsymbol{h}_1, \boldsymbol{h}_2, \ldots, \boldsymbol{h}_M]^{\mathrm{H}}$, $\boldsymbol{s} = [s_1, s_2, \ldots, s_M]^{\mathrm{T}}$, and $\boldsymbol{n} = [n_1, n_2, \ldots, n_m]^{\mathrm{T}}$, respectively. During the beam training procedure, different codewords $\boldsymbol{w}$ are employed sequentially to the UE at different time slots. Based on the received signals, the angle ϕ and the distance r are determined. However, unlike the beam training in the far field which only needs to estimate the angle, the demand of estimating the angle ϕ and the distance r simultaneously requires an unacceptable pilot overhead. Therefore, an effective beam training scheme is essential to fully unleash the benefits of near-field communications.

3 Frequency-dependent focusing based beam training scheme

In this section, we first reveal the frequency-dependent focusing (FDF) property of UCA. Then, based on the FDF property, we design the hierarchical codebook and propose an FDF-based beam training scheme. Finally, we compare the beam training overhead of the proposed FDF-based beam training scheme with those of traditional schemes.

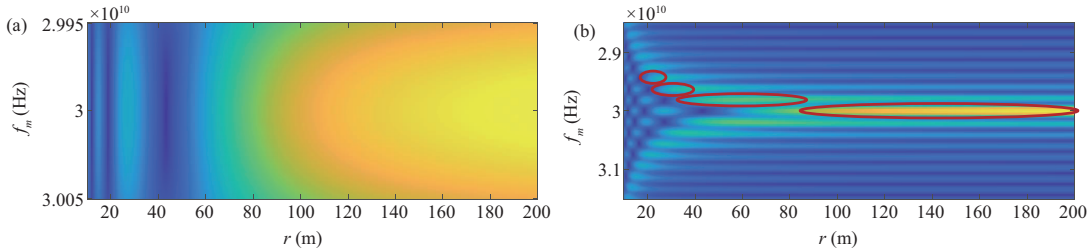

Figure 2 (Color online) Power distribution of UCA when (a) $f_c = 30$ GHz, $B = 100$ MHz and (b) $f_c = 30$ GHz, $B = 3$ GHz.

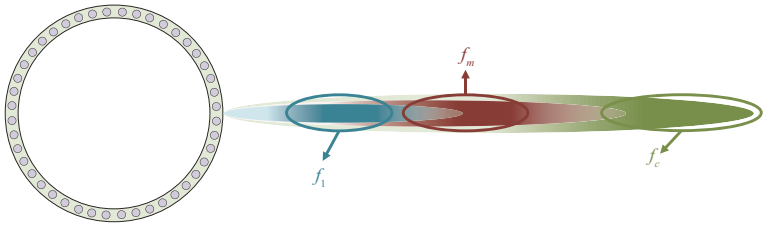

Figure 3 (Color online) Illustration of the frequency-dependent focusing property.

3.1 Frequency-dependent focusing property of UCA

As mentioned above, in ULA systems, the beam split effect can be utilized to improve the beam training efficiency, which inspires us that the wideband effect is common in systems with various antenna array geometries. The wideband effect actually carries more information in the frequency domain, which may be exploited to enhance the beam training performance [30]. In UCA systems, to generate high-gain beams, the beamforming vector $\boldsymbol{w}$ is usually set to the array response vector at the central frequency. Consequently, when the bandwidth is small, as illustrated in Figure 2(a), the beamforming gains at all subcarriers are almost the same. However, in wideband systems, the large bandwidth leads to the mismatch between the beamforming vector and the channels at noncentral frequencies. For example, in wideband UCA systems, high-gain beams cannot form at noncentral frequencies in the far-field, which is called the beam defocus effect [28]. On one hand, the beam defocus effect causes a severe beam gain loss. On the other hand, as illustrated in Figure 2(b), the beams at noncentral frequencies can still focus on a certain distance in the near-field, which is defined as the FDF property in this paper. As marked by the red circles in Figure 2(b), for the subcarriers near the central frequency, the beam power is focused at the far field. When the frequency is far from the central frequency, the focusing distance will be closer to the UCA. To convey the main idea more clearly, we choose 3 typical subcarriers to demonstrate their beam powers in Figure 3. Here, the blue beam represents the beam generated at the subcarrier with the lowest frequency, which focuses at a location very close to the UCA. The dark red beam represents the beam generated at the m-th subcarrier whose frequency is between the lowest frequency and the central frequency. Due to the higher frequency than the blue beam, it focuses at a location further to the UCA. The green beam represents the beam generated at the central subcarrier, which focuses at the far field. By exploiting this property, different distances can be detected by different subcarriers simultaneously, which can significantly reduce the beam training overhead in wideband near-field UCA systems.

To analyze the FDF property, we first derive the beamforming gains of different subcarriers at a certain distance. Specifically, we investigate the beamforming gain at the location (ϕ, r). By setting the beamforming vector $\boldsymbol{w}$ as the far-field array response vector

$$\boldsymbol{w} = \frac{1}{\sqrt{N}} \left[\mathrm{e}^{\mathrm{j}\frac{2\pi R f_c}{c}\cos(\phi-\psi_1)}, \mathrm{e}^{\mathrm{j}\frac{2\pi R f_c}{c}\cos(\phi-\psi_2)}, \ldots, \mathrm{e}^{\mathrm{j}\frac{2\pi R f_c}{c}\cos(\phi-\psi_N)} \right]^{\mathrm{T}}, \tag{6}$$

the beamforming gain at the m-th subcarrier can be calculated as

$$\begin{aligned} G(\boldsymbol{w}, \phi, r, f_m) &\approx \left| \boldsymbol{a}_m^{\mathrm{H}}(\phi, r)\boldsymbol{w} \right| = \frac{1}{N} \left| \sum_{n=1}^{N} \mathrm{e}^{\mathrm{j}\frac{2\pi R}{c}(f_c - f_m)\cos(\phi-\psi_n) + \mathrm{j}\frac{2\pi f_m}{c}\frac{R^2}{2r}\left(1-\cos^2(\phi-\psi_n)\right)} \right| \\ &= \frac{1}{N} \left| \sum_{n=1}^{N} \mathrm{e}^{\mathrm{j}\frac{2\pi R}{c}(f_c - f_m)\cos(\phi-\psi_n) - \mathrm{j}\frac{\pi f_m R^2}{2cr}\cos(2\phi-2\psi_n)} \right|. \end{aligned} \tag{7}$$

Notice that each term in (7) can be replaced by the Bessel functions according to

$$\mathrm{e}^{\mathrm{j}\beta\cos\gamma}=\sum_{\ell=-\infty}^{\infty}\mathrm{j}^{\ell}J_{\ell}(\beta)\mathrm{e}^{\mathrm{j}\ell\gamma}, \tag{8}$$

where $J_\ell(\cdot)$ denotes the ℓ-order Bessel function of the first kind. Then the beamforming gain can be re-written as

$$\begin{aligned}G(\boldsymbol{w},\phi,r,f_m)&=\frac{1}{N}\left|\sum_{n=1}^{N}\left[\sum_{\ell_1=-\infty}^{\infty}\mathrm{j}^{\ell_1}J_{\ell_1}\left(\underbrace{\frac{2\pi R}{c}(f_c-f_m)}_{\beta_1}\right)\mathrm{e}^{\mathrm{j}\ell_1(\phi-\psi_n)}\right]\left[\sum_{\ell_2=-\infty}^{\infty}\mathrm{j}^{\ell_2}J_{\ell_2}\left(\underbrace{-\frac{\pi f_m R^2}{2cr}}_{\beta_2}\right)\mathrm{e}^{\mathrm{j}\ell_2(\phi-\psi_n)}\right]\right|\\&=\frac{1}{N}\left|\sum_{\ell_1=-\infty}^{\infty}\sum_{\ell_2=-\infty}^{\infty}\mathrm{j}^{\ell_1+\ell_2}J_{\ell_1}(\beta_1)J_{\ell_2}(\beta_2)\mathrm{e}^{\mathrm{j}(\ell_1+2\ell_2)\phi}\sum_{n=1}^{N}\mathrm{e}^{-\mathrm{j}(\ell_1+2\ell_2)\psi_n}\right|.\end{aligned} \tag{9}$$

We can replace ψ_n by $\frac{2\pi n}{N}$, and the last summation can be derived as

$$\sum_{n=1}^{N}\mathrm{e}^{-\mathrm{j}(\ell_1+2\ell_2)\psi_n}=\begin{cases}N,\ \ell_1+2\ell_2=N\delta,\delta\in\mathbb{Z},\\0,\ \ \text{else.}\end{cases} \tag{10}$$

According to the inequation that

$$\left|J_{|\ell|}(\beta)\right|\leqslant\left(\frac{\beta e}{2\,|\ell|}\right)^{|\ell|}, \tag{11}$$

the value of the Bessel function is very small and can be neglected when ℓ is large. Thus, when $\ell_1+2\ell_2=N\delta$ and $\delta\neq 0$, though the last summation equals N, $J_{\ell_1}(\beta_1)J_{\ell_2}(\beta_2)\approx 0$ with a large N. Following this approximation, by letting $\ell_1=-2\ell_2=\ell$, Eq. (9) can be further written as

$$G(\boldsymbol{w},\phi,r,f_m)\approx\left|\sum_{-\infty}^{\infty}\mathrm{j}^{-\ell}J_{-2\ell}(\beta_1)J_{\ell}(\beta_2)\right|\overset{\text{(a)}}{=}\left|J_0(\beta_1)J_0(\beta_2)+2\sum_{\ell=1}^{\infty}\mathrm{j}^{-\ell}J_{2\ell}(\beta_1)J_{\ell}(\beta_2)\right|, \tag{12}$$

where (a) is obtained according to $J_\ell(-\beta)=(-1)^\ell J_\ell(\beta)$ and $J_{-\ell}(\beta)=(-1)^\ell J_\ell(\beta)$.

We can observe from Figure 2 that subcarriers with similar frequencies tend to focus on similar distances. By grouping the subcarriers properly, the analysis of the FDF property can be simplified and the wideband UCA system can be more robust to noise during beam training. Thus, based on (12), we propose a subcarrier grouping criterion to divide the subcarriers into several groups, where the subcarriers in a group focus on similar distances. It is worth noting that the beamforming gains at different frequencies reveal periodic fluctuations in the far-field region, which can be exploited to divide the subcarriers into different groups.

Specifically, with $r\to\infty$, $\beta_2\to 0$, and $J_\ell(\beta_2)\to 0$ with $\ell\neq 0$. Thus, Eq. (12) can be simplified as

$$G(\boldsymbol{w},\phi,r,f_m)\approx\left|J_0\left(\frac{2\pi R}{c}(f_c-f_m)\right)\right|. \tag{13}$$

For the zero-order Bessel function of the first kind, the difference between two adjacent zero points approximates π, so the zero points in the frequency domain satisfy

$$\frac{2\pi R}{c}(f_c-f_m)=\pm\left(\frac{1}{2}+s\right)\pi,\quad s=0,1,2,\ldots. \tag{14}$$

Thus, starting from the central frequency, the demarcation frequencies between different groups can be represented according to the zero points as

$$f_d^{(s)}=f_c+\frac{c}{2R}\left(s+\frac{1}{2}\right),\quad s=-\left\lfloor\frac{BR}{c}+\frac{1}{2}\right\rfloor,\ldots,-1,0,1,2,\ldots,\left\lfloor\frac{BR}{c}-\frac{1}{2}\right\rfloor. \tag{15}$$

We divide the subcarriers with frequencies between two demarcation frequencies into one group. Then, all subcarriers can be grouped with the s-th group represented as

$$\mathcal{F}^{(s)}=\left\{f_m \mid f_d^{(s-1)}\leqslant f_m\leqslant f_d^{(s)}, f_m=f_c+\frac{B}{M}\left(m-1-\frac{M-1}{2}\right)\right\}, s=-\left\lfloor\frac{BR}{c}-\frac{1}{2}\right\rfloor,\ldots,\left\lfloor\frac{BR}{c}-\frac{1}{2}\right\rfloor. \tag{16}$$

After grouping all subcarriers, the focusing distances of different groups are analyzed. The focusing distance is defined as the distance with the maximum beamforming gain. For the s-th group, we take the average frequency for analysis, which is formulated as $f_a^{(s)}=\frac{\sum_{f_m\in\mathcal{F}^{(s)}} f_m}{\mathcal{C}_s}$, where $\mathcal{C}_s$ denotes the number of subcarriers in set $\mathcal{F}^{(s)}$. Then, the focusing distance $\hat{r}^{(s)}$ can be obtained by

$$\hat{r}^{(s)}=\arg\max_r\ G(\boldsymbol{w},\phi,r,f_a^{(s)}). \tag{17}$$

Due to the infinite summation, Eq. (17) cannot be solved directly. Fortunately, according to (11), the value of the Bessel function approaches 0 when the order is high. Therefore, a critical problem is determining how many Bessel functions are required to guarantee a good approximation of (17). We notice that the focusing distance becomes shorter as the frequency difference becomes larger, so we propose to analyze the focusing distance sequentially from the central frequency. Specifically, at the central frequency, the beam focuses in the far-field, which means the focusing distance approaches infinity, so only the zero-order Bessel function is needed to obtain a good approximation. When it comes to $\mathcal{F}^{(\pm1)}$, the focusing distance is within the near-field region. To estimate $\hat{r}^{(\pm1)}$, we select the Rayleigh distance, which is utilized to partition the far field and near field to determine the needed order [31]. Rayleigh distance is defined as $r_{\mathrm{RD}}=\frac{2D^2}{\lambda_c}$, where D is the array aperture and $\lambda_c=\frac{c}{f_c}$ is the wavelength at the central frequency. Letting $\beta_2^{(\pm1)}=-\frac{\pi f_a^{(\pm1)}R^2}{2cr_{\mathrm{RD}}}$, the required order $\ell^{(\pm1)}$ can be derived as the maximum integer that satisfies $(\frac{\beta_2^{(\pm1)}e}{2\ell})^\ell\leqslant\Delta$, where Δ is the pre-defined threshold. Then, $G(\boldsymbol{w},\phi,r,f_a^{(\pm1)})$ can be approximated as

$$G(\boldsymbol{w},\phi,r,f_a^{(\pm1)})\approx\left|J_0(\beta_1)J_0(\beta_2)+2\sum_{\ell=1}^{\ell^{(\pm1)}}\mathrm{j}^{-\ell}J_{2\ell}(\beta_1)J_\ell(\beta_2)\right|, \tag{18}$$

and Eq. (17) can be solved by numerical methods such as the Newton-Raphson method. After obtaining $\hat{r}^{(\pm1)}$, the required order $\ell^{(\pm2)}$ of $\mathcal{F}^{(\pm2)}$ can be determined by letting $\beta_2^{(\pm2)}=-\frac{\pi f_a^{(\pm2)}R^2}{2c\hat{r}^{(\pm1)}}$ and solving $(\frac{\beta_2^{(\pm2)}e}{2\ell})^\ell\leqslant\Delta$, and the focusing distances of all groups can then be obtained sequentially.

3.2 Proposed FDF-based beam training scheme

Inspired by the FDF property analyzed above, we propose an FDF-based beam training scheme. Firstly, we design a hierarchical codebook with two layers to explore different angles in space effectively. In the first layer, we divide the UCA into several subarrays, and all subarrays generate directional beams simultaneously to explore a large range of angles in each time slot. To guarantee a relatively high beamforming gain, enough radiation areas are preferred, so in the first layer, each subarray only explores the angles close to its normal direction. As illustrated in Figure 4, we divide the UCA into N_s subarrays. For the n_s-th subarray, the normal direction is $(n_s-\frac{1}{2})\frac{2\pi}{N_s}$, and it only explores angles in range $[(n_s-1)\frac{2\pi}{N_s},n_s\frac{2\pi}{N_s}]$. Then, the angle of each beam needs to be determined. We can view each subarray as a uniform linear array, and the beam width can be approximated as $\varpi_1=\arcsin(2\frac{N_s}{N})$. Thus, the angles of the beams generated by the n_s-th subarray can be formulated as $\vartheta_{n_s}^{(p)}=(n_s-1)\frac{2\pi}{N_s}+(p+\frac{1}{2})\varpi_1, p=0,1,2,\ldots$. Accordingly, the p-th codewords of the first layer can be represented as

$$\boldsymbol{v}_1^{(p)}=\left[\tilde{\boldsymbol{a}}_c^{\mathrm{T}}(\vartheta_1^{(p)},\infty,1),\tilde{\boldsymbol{a}}_c^{\mathrm{T}}(\vartheta_2^{(p)},\infty,2),\ldots,\tilde{\boldsymbol{a}}_c^{\mathrm{T}}(\vartheta_{N_s}^{(p)},\infty,N_s)\right]^{\mathrm{T}},\quad p=0,1,2,\ldots,\left\lceil\frac{2\pi}{N_s\varpi_1}\right\rceil-1, \tag{19}$$

where $\tilde{\boldsymbol{a}}_c(\cdot)$ denotes the operation of selecting the elements corresponding to a certain subarray in vector $\boldsymbol{a}_c(\cdot)$, which can be elaborated as $\tilde{\boldsymbol{a}}_c(\phi,r,n_s)=\boldsymbol{a}_c(\phi,r)[(n_s-1)\frac{N}{N_s}+1:n_s\frac{N}{N_s}]$ with $\boldsymbol{a}_c$ being the array response vector at the central frequency. Based on (19), the codebook of the first layer $\boldsymbol{V}_1$ can be obtained by $\boldsymbol{V}_1=[\boldsymbol{v}_1^{(0)},\boldsymbol{v}_1^{(1)},\ldots,\boldsymbol{v}_1^{(P_1-1)}]$, where $P_1=\lceil\frac{2\pi}{N_s\varpi_1}\rceil$ denotes the necessary overhead for the first-layer

Figure 4 (Color online) Illustration of the designed hierarchical codebook. (a) The first layer; (b) the second layer.

searching. By setting $\boldsymbol{s}$ in (5) as $\mathbf{1}_{M\times 1}$, the received signals corresponding to the first-layer codebook can be formulated as

$$\boldsymbol{Y}_1 = \boldsymbol{H}\boldsymbol{V}_1 + \boldsymbol{N}, \tag{20}$$

where $\boldsymbol{Y}_1 \in \mathbb{C}^{M\times P_1} = [\boldsymbol{y}_1^{(0)}, \boldsymbol{y}_1^{(1)}, \ldots, \boldsymbol{y}_1^{(P_1-1)}]$. Then, the codeword with the maximum received power is selected by

$$\hat{p}_1 = \arg\max_p \left\|\boldsymbol{y}_1^{(p)}\right\|_2. \tag{21}$$

Correspondingly, the UE angle ϕ satisfies

$$\phi \in \bigcup_{n_s=1}^{N_s} \left[(n_s-1)\frac{2\pi}{N_s} + \left(\hat{p}_1 - \frac{1}{2}\right)\varpi_1, (n_s-1)\frac{2\pi}{N_s} + \left(\hat{p}_1 + \frac{1}{2}\right)\varpi_1\right], \tag{22}$$

which determines the searching range of the second-layer codebook.

In the second layer, the entire UCA is utilized to generate beams with high angular resolution to estimate the angle ϕ and the distance r of UE simultaneously. Similarly, we need to determine the angle of each beam first. According to the Lemma 1 in [32], with the beamforming vector being $\boldsymbol{w} = \boldsymbol{a}_c(\phi_1, \infty)$, the beamforming gain at angle ϕ_2 is $|J_0(\frac{4\pi R}{\lambda_c}\sin(\frac{\phi_2-\phi_1}{2}))|$. By setting the threshold as 0.5, the beam width of the second-layer codewords can be approximated as

$$\varpi_2 = 2\arcsin\left(\frac{\lambda_c J_0^{-1}(0.5)}{4\pi R}\right). \tag{23}$$

For the range $[(n_s-1)\frac{2\pi}{N_s} + (\hat{p}_1 - \frac{1}{2})\varpi_1, (n_s-1)\frac{2\pi}{N_s} + (\hat{p}_1 + \frac{1}{2})\varpi_1]$, the number of necessary beams for the second-layer codebook is $P_2 = N_s\lceil\frac{\varpi_1}{\varpi_2}\rceil$. Then, the angle of the p-th beam can be represented as

$$\theta^{(p)} = \left\lfloor\frac{p}{P_1}\right\rfloor\frac{2\pi}{N_s} + \left(\hat{p}_1 - \frac{1}{2}\right)\varpi_1 + \left(\mathrm{mod}(p, P_1) + \frac{1}{2}\right)\varpi_2, \quad p = 0, 1, \ldots, P_2 - 1. \tag{24}$$

Based on (24), the codebook of the second layer can be generated as

$$\boldsymbol{V}_2 = \left[\boldsymbol{a}(\theta^{(0)}, \infty), \boldsymbol{a}(\theta^{(1)}, \infty), \ldots, \boldsymbol{a}(\theta^{(P_2-1)}, \infty)\right], \tag{25}$$

and the received signals corresponding to the second-layer codebook $\boldsymbol{Y}_2 = \boldsymbol{H}\boldsymbol{V}_2 + \boldsymbol{N}$ can be utilized for further process. For the UE angle, by selecting the codeword with the maximum received power by

$$\hat{p}_2 = \arg\max_p \|\boldsymbol{y}_2^{(p)}\|_2,$$

the estimation of UE can be denoted by $\hat{\phi} = \theta^{(\hat{p}_2)}$.

Algorithm 1 Proposed FDF-based beam training scheme

Input: Number of UCA antennas N, number of subarrays N_s, central frequency f_c, bandwidth B, number of subcarriers M, threshold Δ;
Output: Estimated physical location $(\hat{r}, \hat{\phi})$;
1: **Initialization**:
2: Set the focusing distance of the central frequency as $\hat{r}^{(0)} = r_{\mathrm{RD}} = \frac{2D^2}{\lambda_c}$;
3: **for** $s = 1, 2, \ldots, \lfloor \frac{BR}{c} - \frac{1}{2} \rfloor$ **do**
4: $\quad \beta_2^{(\pm s)} = -\frac{\pi f_a^{(\pm s)} R^2}{2c\hat{r}^{(\pm(s-1))}}$;
5: $\quad$ Obtain the required order $\ell^{(\pm s)}$ as the maximum integer satisfying $(\frac{\beta_2^{(\pm 1)} e}{2\ell})^{\ell} \leqslant \Delta$;
6: $\quad$ Determine the focusing distance of the $\pm s$-th group $\hat{r}^{(\pm s)}$ by solving (17);
7: **end for**
8: **Stage I**:
9: Generate the first-layer codebook $\boldsymbol{V}_1$ according to (19);
10: Transmit the codewords in the first-layer codebook and record the received signals: $\boldsymbol{Y}_1 = \boldsymbol{H}\boldsymbol{V}_1 + \boldsymbol{N}$, where $\boldsymbol{Y}_1 = [\boldsymbol{y}_1^{(0)}, \boldsymbol{y}_1^{(1)}, \ldots, \boldsymbol{y}_1^{(P_1-1)}]$;
11: Select the codeword with the maximum received power by (21) and feed back to the BS;
12: **Stage II**:
13: Generate the second-layer codebook $\boldsymbol{V}_2$ based on (25) and the result of the first-layer training;
14: Transmit the codewords in the second-layer codebook and record the received signals: $\boldsymbol{Y}_2 = \boldsymbol{H}\boldsymbol{V}_1 + \boldsymbol{N}$, where $\boldsymbol{Y}_2 = [\boldsymbol{y}_2^{(0)}, \boldsymbol{y}_2^{(1)}, \ldots, \boldsymbol{y}_2^{(P_2-1)}]$;
15: Determine the UE angle by $\hat{\phi} = \theta^{(\hat{p}_2)}$, where $\hat{p}_2 = \arg\max_p \|\boldsymbol{y}_2^{(p)}\|_2$;
16: Group the received signals of all subcarriers based on (26);
17: Determine the UE distance by $\hat{r} = \hat{r}^{(\hat{s})}$ based on (27);
18: **return** $(\hat{r}, \hat{\phi})$.

After determining the UE angle, the UE distance can be estimated based on the FDF property analyzed above. For brevity, let $\tilde{\boldsymbol{y}} = [\tilde{y}_1, \tilde{y}_2, \ldots, \tilde{y}_M]^{\mathrm{T}}$ denote the received signals of the $\hat{p}_2$-th codeword in the second-layer codebook $\boldsymbol{y}_2^{(\hat{p}_2)}$. Then, following the proposed subcarrier grouping criterion, the received signals from different subcarriers are divided into different groups with the s-th group represented as

$$\mathcal{Y}^{(s)} = \left\{ \tilde{y}_m \mid f_m \in \mathcal{F}^{(s)} \right\}. \tag{26}$$

Accordingly, the UE distance is estimated as the focusing distance corresponding to the group with the maximum received power, which can be formulated as $\hat{r} = \hat{r}^{(\hat{s})}$ with $\hat{s}$ represented as

$$\hat{s} = \arg\max_s \frac{\sum_{\tilde{y}_m \in \mathcal{Y}^{(s)}} |\frac{f_c}{f_m} \tilde{y}_m|^2}{\mathcal{C}_s}. \tag{27}$$

The procedure of the proposed FDF-based beam training scheme can be summarized in Algorithm 1. Specifically, in steps 1–7, we initialize the focusing distances of different groups based on the system parameters for beam training. Then, in steps 8–11, we conduct the first-layer searching based on the first-layer codebook and feed the result back to the BS. According to the result of the first-layer searching, the BS generates the second layer codebook in step 13, and transmits the codewords in step 14. Based on the received signals in Stage II, the angle $\hat{\phi}$ and the distance $\hat{r}$ are estimated in steps 15–17, which completes the beam training and the beamforming vector for the UE can be represented as $\boldsymbol{w} = \boldsymbol{a}_c(\hat{\phi}, \hat{r})$.

The proposed scheme can also be extended to multiuser scenarios. Specifically, in the first layer, the UCA transmits the codewords to search for the entire space. Then, for each user, the codeword with the maximum received power is recorded and fed back sequentially to the BS. In the second layer, a finer search is conducted for each user respectively. By this means, each user only needs to feed one additional message back to the BS during the beam training process. Therefore, the proposed scheme can still be applied to multiuser scenarios with a low beam training overhead.

3.3 Pilot overhead analysis

In this subsection, we analyze the pilot overhead of the proposed FDF-based beam training scheme. A comparison is also conducted between the overhead of the proposed scheme and those of hierarchical beam training schemes and exhaustive beam training schemes.

For Stage I, the necessary pilot overhead is $P_1 = \lceil \frac{2\pi}{N_s \varpi_1} \rceil$. When N_s increases, the number of antennas in each subarray decreases, which leads to a larger ϖ_1 and a smaller P_1. For Stage II, the necessary pilot overhead is $P_2 = N_s \lceil \frac{\varpi_1}{\varpi_2} \rceil$, given the fixed number of elements N on UCA, the beam width ϖ_2 is fixed.

Table 1 Pilot overhead comparison

Scheme	$N = 256$	$N = 512$	$N = 1024$
Proposed scheme	61	74	99
Far-field hierarchical scheme	61	74	99
Far-field exhaustive scheme	529	1058	2115
Near-field exhaustive scheme	1058	7406	59220

Table 2 System parameters

Parameter	Value	Parameter	Value
Number of BS antennas N	512	Number of subarrays N_s	8
Central frequency f_c	30 GHz	Parameter Δ	0.1
Bandwidth B	3 GHz	Distribution of path gain g_m	$\mathcal{CN}(0,1)$
Number of subcarriers M	128	Distribution of angle ϕ	$\mathcal{U}(0,2\pi)$

With the increment of N_s, P_2 increases accordingly. Therefore, to realize a low-overhead beam training, the number of subarrays needs to be carefully designed. By approximating $P_1 \approx \frac{2\pi}{N_s\varpi_1}$ and $P_2 \approx N_s\frac{\varpi_1}{\varpi_2}$, the overall pilot overhead for the proposed scheme can be written as $P(N_s) = P_1 + P_2 \approx \frac{2\pi}{N_s\varpi_1} + N_s\frac{\varpi_1}{\varpi_2}$. By letting $P'(N_s) = 0$, the optimal number of subcarriers N_s^{opt} satisfies $N_s^{\text{opt}}\arcsin(2\frac{N_s^{\text{opt}}}{N}) = \sqrt{2\pi\varpi_2}$. It is worth mentioning that the estimation of the distance only utilizes the information carried by different subcarriers, so the proposed beam training scheme requires no extra overhead compared to the far-field hierarchical scheme.

For the far-field exhaustive beam training scheme, $\frac{2\pi}{\varpi_2}$ pilots are required to search the whole space, which is much larger than that of the proposed scheme. In addition, if the near-field propagation is considered, the estimation of distance makes the size of the codebook (e.g., the concentric-ring codebook in [32]) several times larger than that of the far-field exhaustive beam training scheme, which is unacceptable in ELAA systems. In Table 1, we compare the pilot overhead of the proposed scheme when $N_s = 8$ with those of far-field hierarchical scheme, far-field exhaustive scheme, and near-field exhaustive scheme. We can observe that the pilot overheads of the proposed scheme and the far-field hierarchical scheme are low in all scenarios. On the contrary, the exhaustive schemes suffer from an unacceptable overhead when the number of antennas is large, especially the near-field exhaustive schemes.

4 Simulation results

In this section, simulations are conducted to verify the performance of the proposed FDF-based beam training scheme. The system parameters are listed in Table 2. The antenna spacing is set to $d = \frac{c}{2f_c}$, so the radius of UCA R satisfies $R = \frac{d}{2\sin(\frac{\pi}{N})}$. We compare the achievable rate performance of the proposed FDF-based beam training scheme with (1) the optimal solution where the BS knows the perfect CSI, (2) the hierarchical far-field beam training scheme utilizing the same codebook as the proposed scheme, (3) the exhaustive far-field beam training scheme utilizing narrow beam codebook, (4) the exhaustive near-field beam training scheme utilizing the concentric-ring codebook proposed in [32]. In addition, the proposed schemes are also compared with existing beam training schemes in ULA systems, including (5) the exhaustive far-field beam training utilizing DFT codebook, (6) the exhaustive near-field beam training utilizing polar-domain codebook proposed in [33], (7) the hierarchical far-field beam training in [34], and (8) the hierarchical near-field beam training in [14]. The achievable rate is obtained as

$$\mathcal{R} = \frac{1}{M}\sum_{m=1}^{M}\log_2\left(1+\frac{P_t}{\sigma^2}\left\|\boldsymbol{h}_m^{\mathrm{H}}\boldsymbol{w}\right\|^2\right) = \frac{1}{M}\sum_{m=1}^{M}\log_2\left(1+\frac{P_tNg_m^2}{\sigma^2}\left\|\boldsymbol{a}_m^{\mathrm{H}}(\phi,r)\boldsymbol{w}\right\|^2\right), \tag{28}$$

where $\frac{P_tNg_m^2}{\sigma^2}$ is defined as the signal-to-noise ratio (SNR).

Figure 5(a) reveals the achievable rate performance against the SNR. The distance between the BS and the UE satisfies the uniform distribution $r \sim \mathcal{U}(5\text{ m}, 20\text{ m})$, the beam training overhead is set to 128, and the SNR increases from -5 to 15 dB. We can observe that in all considered scenarios, the achievable rate performance of the proposed scheme is higher than that of other schemes since the proposed scheme can exploit the large bandwidth in wideband systems to estimate the angle and the UE

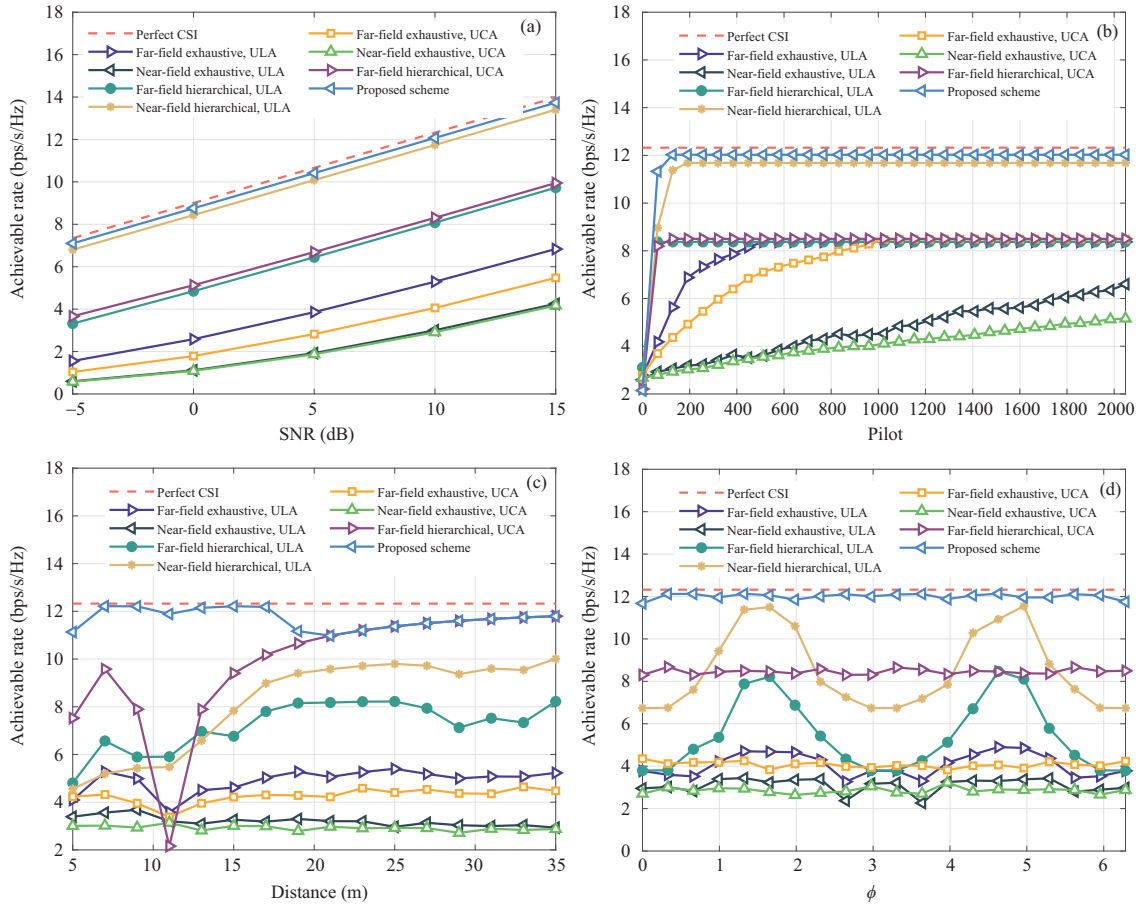

Figure 5 (Color online) Achievable rate performance against (a) SNR, (b) pilot overhead, (c) the distance between the BS and the UE, and (d) the UE angle ϕ.

distance simultaneously with a low pilot overhead. For the far-field hierarchical beam training scheme, only the UE angle can be detected, so the lack of distance information leads to a lower achievable rate. For the two exhaustive schemes, since the beam training overhead is not sufficient, the location of UE cannot be estimated correctly in most cases. Thus, the achievable rates of these two schemes are much lower than those of the two hierarchical schemes. For schemes in ULA systems, since the codebook size of ULA is a little smaller than that of UCA, there exists a slight gap between the far-field exhaustive schemes of ULA and UCA. For the hierarchical schemes, since the beams generated by UCA are a little narrower than those generated by ULA, the achievable rates in UCA systems are a little bit higher than those in ULA systems.

To illustrate the impact of pilot overhead, we compare the achievable rate performance of different schemes under different pilot overheads in Figure 5(b). The beam training SNR is set to 10 dB, the distance between the BS and the UE satisfies the uniform distribution $r \sim \mathcal{U}(5\text{ m}, 20\text{ m})$, and the pilot overhead increases from 0 to 2048. Due to the high efficiency of the hierarchical codebook, the achievable rate performance of the proposed scheme and the far-field hierarchical scheme reaches their peaks when the overhead is around 100, and the proposed scheme realizes a more accurate beam training by considering the spherical wavefront in the near-field scenarios. This phenomenon also verifies the aforementioned clarity that the proposed scheme requires no extra pilot overhead compared to far-field schemes. On the contrary, for exhaustive schemes, the achievable rate performance is severely limited due to the unacceptable beam training overhead. For example, the far-field exhaustive beam training scheme reaches its best performance when the overhead is around 1000, which is consistent with Table 1, while for the near-field exhaustive beam training scheme, the pilot overhead is far from sufficient in all considered overhead configurations, which leads to a worse achievable rate performance. It is worth noting that when the pilot length is 0, the achievable rates of the exhaustive schemes are a little bit higher than those of hierarchical schemes. This phenomenon is related to the detailed beam training strategy when

the pilot overhead is not sufficient. When the pilot overhead is 0, we just choose a random codeword as the beamforming vector. Since the beam gains of the exhaustive codewords are much higher than those of hierarchical codewords, although the beam coverages are also different, the statistical performances may vary slightly. For schemes in ULA systems, the curve of the far-field exhaustive scheme further verifies the codebook size of ULA is smaller than that of UCA. It is also revealed that the necessary pilot overheads of the hierarchical schemes are similar in both systems.

The achievable rate performance against the distance between the BS and the UE is also demonstrated in Figure 5(c). The SNR is set to 10 dB, the pilot overhead is set to 128, and the distance increases from 5 to 35 m. It can be observed that the proposed scheme reaches the highest achievable rate performance in all considered distances. When the distance is around 20 m, the proposed scheme experiences a slight performance degradation. This is because the distance sampling around 20 m is relatively rough, which leads to a larger error. In spite of this, the proposed scheme still outperforms all other schemes in distances around 20 m. It is also worth noting that the far-field hierarchical beam training scheme suffers from a severe performance loss around 11 m. This is due to the serious mismatch between the far-field array response vector and the near-field channel around 11 m. As the distance increases, the performance gap between the proposed scheme and the far-field hierarchical scheme approaches zero since the spherical propagation effect is slight. For two exhaustive schemes, the achievable rate performance remains low due to the insufficient pilot overhead. For the exhaustive schemes in ULA systems, since the codebook size of ULA is smaller than that of UCA, the achievable rate in ULA systems is relatively higher than that in UCA systems. For the hierarchical schemes, the performance gap between ULA systems and UCA systems is relatively large. This is because in most angles, the effective array aperture of ULA is larger than that of UCA, which results in a larger near-field range. In this case, the performance in ULA systems improves slower than that in UCA systems.

We also compare the achievable rate performance against the UE angle ϕ in Figure 5(d). The SNR is set to 10 dB, the pilot overhead is set to 128, the distance between the BS and the UE satisfies the uniform distribution $r \sim \mathcal{U}(5 \text{ m}, 20 \text{ m})$, and the UE angle is uniformly sampled in $[0, 2\pi]$. It is revealed that due to the axial symmetry of UCA, all considered schemes can achieve a relatively fair achievable rate performance at different angles. For two hierarchical schemes, the proposed scheme outperforms the far-field scheme by estimating the angle and the UE distance simultaneously. For two exhaustive schemes, due to the insufficient beam training overhead, the achievable rate performance is severely limited. For schemes in ULA systems, we can notice that since the effective array aperture of ULA is different at different angles, the performance of schemes in ULA systems also varies accordingly. Specifically, when the angle ϕ is near the end-fire, the effective array aperture is small, making the near-field range small. In this case, the achievable rates are high. On the contrary, when the angle ϕ is near the normal direction, the achievable rate performance is lower. This is because the near-field range is large, so the codebook sampling near the antenna array is not accurate.

In addition, we illustrate the impact of the number of subarrays N_s on the beam training performance of the proposed scheme in Figure 6. In our considered scenario, $N_s^{\text{opt}} \approx 7.04$. Therefore, when $N_s = 8$, the achievable rate performance reaches its peak at first. On the contrary, when the number of subarrays is smaller ($N_s = 4$) or larger ($N_s = 12, 16$), the achievable rate performance improves slower, which verifies the analyses in Subsection 3.3. Meanwhile, we can notice that the beam training accuracy is almost the same regardless of the number of subarrays. This is because in the second layer, the directional beam is always generated by the entire UCA, which bears no relation to N_s.

In summary, the proposed FDF-based beam training scheme can realize an accurate beam training with a low pilot overhead. By estimating the angle effectively with the hierarchical codebook and estimating the distance based on the received signals at different subcarriers, the location of UE in the near-field can be detected accurately with a low beam training overhead. Compared with existing schemes in ULA systems, due to the axial symmetry of UCA, the performance of the proposed scheme is more consistent.

5 Conclusion

In this paper, we investigated the effective beam training in near-field wideband UCA systems. Specifically, we first analyzed the frequency-dependent focusing property in wideband UCA systems, where subcarriers at different frequencies focused on different distances. By exploiting this property, different distances in the near field could be searched simultaneously by different subcarriers. Then, we designed

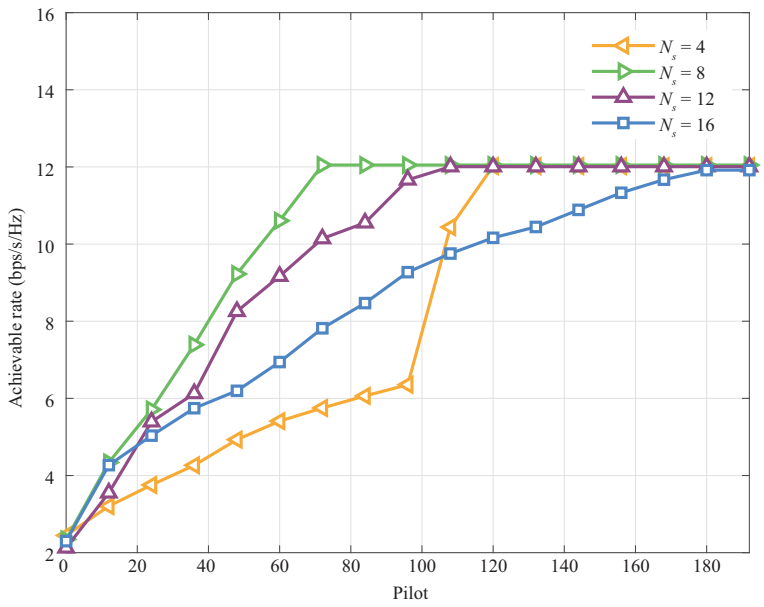

Figure 6 (Color online) Achievable rate performance comparison of the different numbers of subarrays.

a hierarchical codebook and proposed the corresponding FDF-based beam training scheme to realize an accurate beam training with a low beam training overhead. In addition, a comparison was made between the beam training overhead of the proposed scheme and those of existing schemes. Finally, simulation results verified the effectiveness of the proposed scheme. The proposed scheme established the relationship between the subcarrier frequency and the UE distance in the near-field wideband ELAA systems with UCA, which could be utilized to reduce the pilot overhead for CSI acquirement in various scenarios. For future work, the FDF property revealed in this paper may be extended to other near-field UCA scenarios, such as reconfigurable intelligent surface (RIS) communications and cell-free mMIMO communications.

Acknowledgements This work was supported by National Key Research and Development Program of China (Grant No. 2023YFB3811503).

References

1 Rappaport T S, Sun S, Mayzus R, et al. Millimeter wave mobile communications for 5G cellular: it will work! IEEE Access, 2013, 1: 335–349
2 Rappaport T S, Xing Y, Kanhere O, et al. Wireless communications and applications above 100 GHz: opportunities and challenges for 6G and beyond. IEEE Access, 2019, 7: 78729–78757
3 Wang Y P, Chen X M, Pei H L, et al. MIMO performance enhancement of MIMO arrays using PCS-based near-field optimization technique. Sci China Inf Sci, 2023, 66: 162302
4 Elayan H, Amin O, Shihada B, et al. Terahertz band: the last piece of RF spectrum puzzle for communication systems. IEEE Open J Commun Soc, 2020, 1: 1–32
5 Ning B, Tian Z, Chen Z, et al. Prospective beamforming technologies for ultra-massive MIMO in Terahertz communications: a tutorial. 2021. ArXiv:2107.03032
6 Kürner T, Ke G, Molisch A, et al. Millimeter wave and THz propagation channel modeling for high data rate railway connectivity—status and open challenges. ZTE Commun, 2016, 14: 7–13
7 Jiang H, Dai L L. Transformer-based downlink precoding design in massive MIMO systems for 5G-advanced and 6G. Sci China Inf Sci, 2023, 66: 199301
8 Wu W, Liu D, Hou X, et al. Low-complexity beam training for 5G millimeter-wave massive MIMO systems. IEEE Trans Veh Technol, 2020, 69: 361–376
9 Ali A, González-Prelcic N, Heath R W. Millimeter wave beam-selection using out-of-band spatial information. IEEE Trans Wireless Commun, 2018, 17: 1038–1052
10 Piesiewicz R, Kleine-Ostmann T, Krumbholz N, et al. Short-range ultra-broadband Terahertz communications: concepts and perspectives. IEEE Antennas Propag Mag, 2007, 49: 24–39
11 Cui M, Dai L, Schober R, et al. Near-field wideband beamforming for extremely large antenna array. 2021. ArXiv:2109.10054
12 Cui M, Wu Z, Lu Y, et al. Near-field MIMO communications for 6G: fundamentals, challenges, potentials, and future directions. IEEE Commun Mag, 2023, 61: 40–46
13 Wei X, Dai L, Zhao Y, et al. Codebook design and beam training for extremely large-scale RIS: far-field or near-field? China Commun, 2022, 19: 193–204
14 Lu Y, Zhang Z, Dai L. Hierarchical beam training for extremely large-scale MIMO: from far-field to near-field. IEEE Trans Commun, 2024, 72: 2247–2259
15 Shi X, Wang J, Sun Z, et al. Spatial-chirp codebook-based hierarchical beam training for extremely large-scale massive MIMO. IEEE Trans Wireless Commun, 2024, 23: 2824–2838

16 Zhang Y, Wu X, You C. Fast near-field beam training for extremely large-scale array. IEEE Wireless Commun Lett, 2022, 11: 2625–2629
17 Liu W, Ren H, Pan C, et al. Deep learning based beam training for extremely large-scale massive MIMO in near-field domain. IEEE Commun Lett, 2023, 27: 170–174
18 Meng F, Huang Y M, Lu Z H, et al. Multi-user mmWave beam tracking via multi-agent deep Q-learning (in Chinese). ZTE Commun, 2023, 21: 53–60
19 Cui M, Dai L, Wang Z, et al. Near-field rainbow: wideband beam training for XL-MIMO. IEEE Trans Wireless Commun, 2023, 22: 3899–3912
20 Cui M Y, Dai L L. Near-field wideband channel estimation for extremely large-scale MIMO. Sci China Inf Sci, 2023, 66: 172303
21 Tewfik A H, Hong W. On the application of uniform linear array bearing estimation techniques to uniform circular arrays. IEEE Trans Signal Process, 1992, 40: 1008–1011
22 Kallnichev V. Analysis of beam-steering and directive characteristics of adaptive antenna arrays for mobile communications. IEEE Antennas Propag Mag, 2001, 43: 145–152
23 Chan S C, Chen H H. Uniform concentric circular arrays with frequency-invariant characteristics theory, design, adaptive beamforming and DOA estimation. IEEE Trans Signal Process, 2007, 55: 165–177
24 Zhang F, Fan W, Pedersen G F. Frequency-invariant uniform circular array for wideband mm-Wave channel characterization. Antennas Wirel Propag Lett, 2017, 16: 641–644
25 Wu Z, Cui M, Zhang Z, et al. Distance-aware precoding for near-field capacity improvement. 2021. ArXiv:2112.14598
26 Wu Z, Dai L. Multiple access for near-field communications: SDMA or LDMA? IEEE J Sel Areas Commun, 2023, 41: 1918–1935
27 Xie Y, Ning B, Li L, et al. Near-field beam training in THz communications: the merits of uniform circular array. IEEE Wireless Commun Lett, 2023, 12: 575–579
28 Wu Z, Dai L. The manifestation of spatial wideband effect in circular array: from beam split to beam defocus. 2023. ArXiv:2305.02875
29 Tang W, Chen M Z, Chen X, et al. Wireless communications with reconfigurable intelligent surface: path loss modeling and experimental measurement. IEEE Trans Wireless Commun, 2021, 20: 421–439
30 Chen Y, Tan J, Hao M, et al. Accurate beam training for RIS-assisted wideband Terahertz communication. IEEE Trans Commun, 2023, 71: 7425–7440
31 Sherman J. Properties of focused apertures in the fresnel region. IRE Trans Antennas Propag, 1962, 10: 399–408
32 Wu Z, Cui M, Dai L. Enabling more users to benefit from near-field communications: from linear to circular array. IEEE Trans Wireless Commun, 2024, 23: 3735–3748
33 Cui M, Dai L. Channel estimation for extremely large-scale MIMO: far-field or near-field? IEEE Trans Commun, 2022, 70: 2663–2677
34 Noh S, Zoltowski M D, Love D J. Multi-resolution codebook and adaptive beamforming sequence design for millimeter wave beam alignment. IEEE Trans Wireless Commun, 2017, 16: 5689–5701